RSC Advances

ROYAL SOCIETY OF CHEMISTRY

www.rsc.org/advances

Hydrothermal Synthesis of Hardened Diatomite-based Adsorbents with Analcime Formation for Methylene Blue Adsorption

Zhang Yi[1], Jing Zhenzi[1], Tomohito Kameda[2], Toshiaki Yoshioka[2]*

[1] Key Laboratory of Advanced Civil Engineering Materials,

Ministry of Education, Tongji University, China

[2] Graduate School of Environmental Studies, Tohoku University, Japan

ABSTRACT: A facile hydrothermal method has been developed to synthesize natural diatomite into hardened diatomite-based adsorbents with zeolite (analcime) formation for methylene blue(MB)adsorption. The results showed that the initial and final strengths were provided with the formed C-S-H gel and zeolite (analcime), respectively. Due to the low temperature synthesis, the formed analcime and retained diatomite were also found to exert a synergistic effect on MB adsorption. The NaOH concentration had a significant effect on the C-S-H and analcime formations, and a lower NaOH concentration (≤9 M) was favorable to C-S-H gel formation, while analcime formed readily at a higher NaOH concentration (≥12 M). The curing temperature and time also influenced the formation of analcime, a long curing time (≥12 h) or a high temperature

(≥473 K) was favorable to analcime formation, while an overlong time (≥24h) or over-high temperature (≥493 K) had a minus effect on the strength of the specimens. The adsorption of MB in this study followed pseudo-second-order kinetics, with a maximum adsorption capacity of 129.87 $mg \cdot g^{-1}$ at 308 K, according to the Langmuir model. Thermodynamic studies also showed that the adsorption process was spontaneous and endothermic. As such, tough diatomite-based adsorbents with analcime formation could be synthesized hydrothermally, which could be used to capture MB in wastewater efficiently.

1. INTRODUCTION

Dyes are commonplace in modern society, with more than 100,000 compounds of dyes is employed in the plastics, textile, dye, paper, and printing industries[1], and these dye effluents have constituted a worldwide environmental pollution problem because of their huge volumes.[2] Dyes are highly visible, and even trace in water[3] will potentially prevent light penetration, which has a negative impact on aquatic life. [4] Furthermore, they are also potentially carcinogenic and/or toxic to human being.[5] The capture of dye in wastewater is therefore a critical and urgent issue. Many methods have been proposed for the elimination and removal of dye, e.g. adsorption,[3] membrane separation[6], electrochemical degradation,[7] and microbial decolorization.[8] Among them, adsorption is currently considered as the most favored approach because of its cost-effectiveness and simplicity.

Diatomite, with the high porosity and permeability, large surface area, and chemical inertness,[9] has been widely used for wastewater treatment.[10] Similarly, zeolites,–a family of hydrated microporous aluminosilicate, because of the properties of minerals-offering cation exchange, molecular sieving, and sorption properties[11], have been also used as effective adsorbents of dye from wastewater.[12] Some studies therefore, have focused on the preparation of zeolites or zeolite/diatomite composites from diatomite for wastewater treatment.[9, 13, 14] However, the prepared materials were commonly used as the fine powder form, which has an unavoidable drawback for

further applications because both more sewage sludge is produced and the used materials are also difficult to recycle. For this reason, how to produce a tough adsorbent is very important. The tough materials could be prepared with diatomite by high-temperature (≥900 °C) sintering,[15, 16] and however this might destroy the original microporous structure of the raw material (diatomite) readily because clay-based products should be manufactured at temperatures below 500 °C to retain their inherent property and performance.[17] Under hydrothermal conditions, the ion product constant of water is thousands times higher than that at standard pressure and temperature, and thus the low temperature(≤473K) hydrothermal solidification(a dissolution/precipitation process) technology might have a capability of not only producing a tough specimen but also retaining the inherent properties of raw material. Previously, our preliminary researches[18, 19] have showed that tough and porous materials could be obtained hydrothermally with tobermorite or analcime formation. However, a detailed presentation, i.e., preparing a hardened diatomite-based adsorbent and further evaluating its adsorption of dye from wastewater, has not been reported extensively in literature.

Therefore, this work tried to hydrothermally solidify (≤473K) diatomite with zeolite (analcime) formation, for which the analcime formation can enhance the mechanical strength of diatomite specimens, and moreover both the retained diatomite and formed analcime can exert synergistic effects on the adsorption for dyes. The objectives of this

work were (i) to enhance the strength of the diatomite specimen via a hydrothermally formed zeolite and investigate the hardening mechanism; (ii) to study the effects of the sodium hydroxide concentration and the duration time and temperature of the hydrothermal treatment on the phase evolution and the strength development of the specimens; (iii) to investigate the capacity for MB adsorption of the diatomite based material, and (iv) to characterize the adsorption mechanism.

2. EXPERIMENTAL SECTION

2.1. Materials

Natural diatomite, obtained from Shengzhou Shuiquan Diatomite Product (Zhejiang, China), was first crushed to pass 350-mesh sieve, and then used as a raw material without any pretreatment. Sodium hydroxide and MB (analytical grade) were obtained from Sinopharm Chemical Reagent (Shanghai, China). Double distilled water was used throughout in this study.

2.2. Synthesis

Diatomite mixed with 10 wt.% calcium hydroxide, was used as a starting material. The staring materials was first mixed with 20 wt.% sodium hydroxide(NaOH) at different concentrations (viz. 6 M, 9 M, 12 M, and 15 M), and then the specimens uniaxially compacted by a pressure of 20 MPa. The demolded specimens (40 mm × 15 mm × 8 mm) were subsequently treated hydrothermally at 373–493 K under saturated steam pressure (0.1–1.55 MPa) for up to 24 h. The Teflon-lined stainless steel hydrothermal

apparatus used in this study is accordance with our previous described method.[20] All the specimens were air-dried at 353 K for 24 h and subsequently stored in desiccators for further study.

2.3. Characterization

The flexural strength of the dried specimens was measured on a universal testing machine (Xie Qiang Instrument Technology, XO-106A) using the three-point method, at a loading rate of 0.5 mm·min^{-1}. The values reported here were the means of three measurements performed on the three specimens taken from each mixture. The chemical composition of the specimens was determined by X-ray fluorescence spectroscopy (XRFS, SRS3400, Bruker); the crystal phases were identified by powder X-ray diffraction (XRD), performed on a diffractometer (Rigaku D/max-rB) with Cu Kα radiation, running at 40 kV and 30 mA, and scanning 2θ from 5° to 70°; the microstructures and morphological characteristics of the specimens were investigated by environmental scanning electron microscopy (SEM, Quanta, 200FEG) combined with energy dispersive X-ray spectroscopy (EDX, Genesis X4 M, EDAX);the mid-infrared spectra (IR) of the specimens(4000-400 cm^{-1}) were recorded on a FT-IR spectrometer (Nicolet 6700, Thermo Scientific) using KBr discs prepared by mixing 1% of the finely ground sample in KBr for functional groups analysis; nitrogen gas sorption analysis was performed at 77 K using an automated system (Nova2000e, Quantachrome) for the specific surface area and the mesoporous size distribution; the mercury intrusion

porosimetry was applied to measure the pore characteristics of specimens using an automatic equipment(AutoPoreIV 9510, Micromeritics), allowing for the intrusion of mercury into pores with diameters ranging between 403 μm for minimal pressure(0.54 psi) and 3.8 nm for the maximum pressure(59951 psi); the cation-exchange capacity (CEC) of samples was investigated according to the standard of American Society for Testing and Materials (ASTM D7503-10).

2.4. Adsorption Experiments

The crushed specimens were sieved through -40+80 mesh, washed with distilled water to remove possible unreacted sodium/calcium hydroxide, and dried at 353 K until reaching a constant weight. Adsorption experiments were performed at 288, 298, and 308 K in a set of 150 ml conical flasks. The specimens (1 g) were added to MB solutions (100 ml, 250, 500 or 1000 ppm, natural pH); the flasks were then sealed and placed in thermostatic shaker operated at 120 rpm until equilibrium was attained. At a given time, the MB solution was withdrawn and separated by centrifugation at 5000 rpm for 10 min. The supernatant was collected and characterized by UV-visible spectrophotometry (INESA, UV765) at 664 nm. The adsorption capacity (q_e) of the specimens for MB and the efficiency of its removal were then calculated using

$$q_e = (C_0 - C_e)V / M \quad (1)$$

where q_e (mg·g^{-1}) is the equilibrium adsorption capacity, C_0 and C_e are respectively the initial and equilibrium MB concentrations (mg·L^{-1}), V (L) is the volume of the solution, and M (g) is the mass of the adsorbent.

3. RESULTS AND DISCUSSION

3.1. Characterization of Diatomite

The chemical and mineral components of diatomite have a significant influence on the hydrothermal synthesis analcime for strength enhancement. The main chemical composition of the raw diatomite is SiO_2, 66.7wt. %; Al_2O_3, 15.3wt.%; Fe_2O_3, 6.32wt.%; K_2O,2.09wt.%, with a small amount of MgO, CaO, MnO and TiO_2. It should be noted that the SiO_2/Al_2O_3 molar ratio of the diatomite is about 7, which is considered to be appropriate for synthesis of low-Si zeolite with natural clay materials.[21, 22] Figure 1 shows that the main mineral components of diatomite are quartz (SiO_2, JCPDS# 46-1045), montmorillonite ($Na_{0.3}(Al,Mg)_2Si_4O_{10}(OH)_2 \cdot 8H_2O$, JCPDS# 29-1499) and Kaolinite ($Al_4(OH)_8(Si_4O_{10})$, JCPDS# 99-0067). A broad reflection background related to the amorphous silica structure of diatomite was also observed approximately at 19-30^o(2θ) which overlapped with some peaks of above identified minerals, in good agreement with that of the referenced typical diatomite.[23] The functional group of diatomite was identified by FTIR analysis. As shown in Figure 2, the bands at 3699 and 3621 cm^{-1} correspond to the vibration of the surface hydroxyls(-OH) group and inner hydroxyl group on the clay(diatomite),[24] the broad band centered at 3423 cm^{-1} and the

band at 1635cm^{-1} to the O-H vibration of the physically adsorbed water and the structural water, respectively;[25] the bands at 1105 and 1035 cm^{-1}(strong and broad) correspond to siloxane(Si-O-Si) stretching;[26] the band at 798 cm^{-1} is a response to an intertetrahedral Si-O-Si bending vibration, and the bands at 694 and 468 cm^{-1} are due to O-Si-O bending vibration;[27] the bands of low intensity observed at 914 and 534 cm^{-1} are assigned to the Si(Al)-O-Al vibration and suggests the presence of the other mineral clay[28] (kaolinite, montmorillonite) in diatomite, which is good consistent with the XRD analysis .

3.2 Synthesis of zeolite

The ideal chemical equation for the synthesis of analcime ($NaAlSi_2O_6 \cdot H2O$) can be described by the following equation:

$$2NaOH(aq) + 4SiO_2(s) + Al_2O_3(s) \rightarrow 2NaAlSi_2O_6 \cdot H_2O(s) \quad (2)$$

The Si and Al source can be provided with diatomite, while the added NaOH solution can both supply the Na source and improve the reactivity because the reactivity depends mainly on the dissolution of quartz, and NaOH has primary impact on dissolution of quartz and kaolinite for analcime zeolite precipitation.[22]

3.2.1 Effect of the NaOH Concentration

Figure 3 shows the strength development with NaOH concentration of the specimens cured at 473 K for 12 h. The flexural strength increased with the NaOH concentration up to 12 M, and then decreased thereafter.

The XRD patterns of the above specimens are also shown in Figure 4. Compared with peaks of raw diatomite (Dia.), a broad band near 30° indexed to C-S-H (JCPDS#33-0306) appeared from 6M NaOH but disappeared at 12 M. At the same time, distinct peaks corresponding to analcime (JCPDS#99-0007) were observed at 12 M NaOH, which suggests that a higher alkaline was favorable to analcime formation. Comparison of phase evolution (Figure 4) with strength development (Figure 3) shows that the initial strength enhancement at low alkaline (6 M,9 M) was mainly due to C-S-H gel formation, while the further strength development was depended on the analcime formation at a high alkaline (12 M). Because the OH- provided by NaOH solution has great capability of dissolving the amorphous silicate and kaolinite through breaking the Si-O and Al-O bonds under hydrothermal conditions. The dissolved species, e.g. $[H_2SiO_4]^{2-}$, $[H_3SiO_4]^-$ and $[Al(OH)4]^-$, around the diatomite particles favored to react with Ca^{2+} and OH^- to form C-S-H gel. Before the hydrothermal processing, the starting material was only compacted, however, the formed cross-linking C-S-H could fill in the spaces between diatomite particles as binder after hydrothermal processing which densified the matrix and thus provided the initial strength enhancement. As mentioned above, NaOH solution plays double roles in this study, i.e. the improvement of reactivity and provision of Na source to form analcime. At a higher NaOH concentration (12 M), because the surface charge of diatomite is normally negative via deprotonation process ($\equiv XOH \leftrightarrow \equiv XO^- + H^+$), the Na^+ ion is inclined to be concentrated on the surface of the

particles. For this reason, quartz favors to be dissolved into free Si-O tetrahedron to form analcime with the enriched Na^+ around the particles. The formed analcime grew between particles and therefore significantly improved the strength of the specimen (Figure 13c). The hydrothermally solidified materials could be taken as complex multiphase inhomogeneous phases which consist of unreacted diatomite particles (crystalline quartz), formed crystal phases (analcime/C-S-H) and the interface zone between them. Crystalline quartz herein plays a main role on the strength of the specimen because it is regarded as both aggregate and the matrix framework. The formed crystals, which deposits on the surfaces of particles, can fill in the interface zones (spaces) of matrix as a function of binder. At higher NaOH concentration (15 M), although more analcime could be formed, more dissolution of quartz in diatomite particles seemed to result in the framework looser inevitably, which in turn reduced the strength eventually.

Figure 5 shows the FTIR spectra of the above specimens. The peak at 1440cm^{-1} referring to asymmetric vibration of CO_3^{2-} is probably due to the carbonation during synthesis and preparation of IR specimens. The peak at 3700 cm^{-1} (surface hydroxyls) disappeared while the peak at 3621 cm^{-1}(inner hydroxyls) reserved with NaOH additions, which confirmed that the dissolution of Si(Al)-OH structure normally occurred on the surface of the diatomite particles, and the original microporous structure (inner hydroxyls) of the raw material(diatomite) could be retained after low temperature

hydrothermal treatment. The peaks at 914 cm^{-1} corresponding to kaolinite disappeared after NaOH was added. The intensity of peaks at 694 cm^{-1} and 468 cm^{-1} referred to the O-Si-O vibration decreased, suggesting that more quartz dissolved at higher alkaline. At 12 M, 15 M, the IR wavenumbers revealed analcime formed, in agreement with previous research.[22]

3.2.2. Effects of the Hydrothermal Temperature

Figure 6 shows that the flexural strength development of the specimens cured for 12 h with 12 M NaOH at different curing times, and the strength increased until the curing temperature of 473 K, then decreased slightly. The maximum flexural strength at 473 K was 17 MPa.

The XRD patterns of these specimens (Figure 7) shows that at 423 K some peaks corresponding to C-S-H and portlandite due to $Ca(OH)_2$ addition appeared compared to that of raw diatomite. This suggests that even at low temperature (423 K), some dissolved amorphous silicate could provide $[H_2SiO_4]^{2-}$ species to formed C-S-H with Ca^{2+} and OH^- which enhanced the initial strength of specimens. With increasing curing temperature, the ion-product constant of water increased greatly and then accelerated the destruction of tetrahedron structure via breaking of Al-O (kaolinite) and hydrolysis of Si-O-Si[22] (quartz, amorphous silicate), which favored to form analcime, in turn enhanced the strength of the specimens. Although analcime could also form at 493 K, the over-dissolution of crystalline quartz loosed the matrix and then led to the reduction

in strength shown in Figure 6. Figure 8 shows the FTIR spectra of the above specimens. The peak at 3700 cm^{-1}(surface hydroxyl) and 914 cm^{-1}(Kaolinite) could be observed at 373 K and then disappeared at higher curing temperature; the peaks at 694 cm^{-1} and 468 cm^{-1} attributed to O-Si-O vibration decreased with increasing temperature, and the typical IR peaks of analcime could be also observed in the specimens at curing temperature of 473K and 493 K, respectively.

3.2.3. Effects of the Hydrothermal Time

Figure 9 shows that the flexural strength of the specimens increased gradually with the curing times of the specimens cured at 473 K with 12 M, reached a maximum flexural strength of 17 MPa at 12 h, and afterward decreased slightly.

The XRD patterns of these specimens (Figure 10) reveal that an increase in the synthesis times from 1 to 6 h led to disappearance of the amorphous silicate and kaolinite phases, while a weak C-S-H peak became discernible. Phase corresponding to analcime was observed for longer curing times from 12 to 24 h. FTIR spectra (Figure 11) of these specimens also reveals a similar result with that of XRD analysis, that is, the peaks referred to O-Si-O vibration (694,468 cm^{-1}) decreased. Comparison of the evolution of these phases with the development of the strength of the corresponding specimens suggests that C-S-H contributed to the initial strength enhancement, while the final strength development stemmed from the analcime formation. However, overlong times (> 12 h) and over high temperature (> 473 K) seemed to have a

negative impact on the strength development. There are two possible factors that may have negative effects on strength development: (1) the over-dissolution of crystalline quartz in diatomite particles, and (2) The over-growth of the formed crystals. The larger crystals might cause the structural change, internal stress and loose matrix, thus leading to a reduction in strength, in agreement with our previous work.[29, 30]

3.2.4. Evolution of the Porosity.

. Figure 12 shows the evolution of the porosity within matrix with increasing curing time. Before hydrothermal treatment (without curing), the pore had a broad size distribution between 0.02 μm and 1.5 μm corresponding to the voids between diatomite particles in the green specimens, and a fine pore distribution (<10 nm) also appeared which should attribute to the inherent microstructure of diatomite (Figure 13a). At 1h, there only was a small change for the pore size distribution compared with that without hydrothermal processing, suggesting a small reaction occurred within the matrix during hydrothermal processing. At 6 h, the peak intensity (0.02-1.5 μm) decreased and a broad pore size distribution at 4-100 nm tended to appear, reflecting that some reactions have happened and some diatomite has been consumed within matrix. The SEM micrograph of the specimen cured at 6 h (Figure 13b) indicated that the newly formed cross-linking C-S-H was filled in the voids of diatomite particles and the intercrystalline pores of formed C-S-H led to the fine pore peak (4-100 nm). The formed C-S-H gel also enhanced the strength (Figure 9). At 12 h, more fine pores (2-20 nm) were

formed because of a higher pore size distribution peak, which suggests that more crystals formed in matrix. The SEM micrograph (Figure 13c) and EDS analysis show that the formed crystal was mainly analcime. It should be noted that diatomite still survived in matrix (Figure 13c), and this might be the reason that the specimen at 12 h had a similar pore size distribution of (0.02-1.5 μm) with that of the diatomite (due to low temperature curing, the reaction only occurs on the surface of diatomite so that the microstructure within diatomite (particles) is not destroyed). For a long curing time (24 h), however, the fine pore size distribution tended to disappear and main peak of the pore size distribution (0.02-1.5 μm) shifted to larger pore size, suggesting that the small crystals (fine intercrystalline pores) have grown very largely. This also made the matrix loose (Figure 13d), and in turn led to the strength reduction shown in Figure 9. It is notable that much more fine pores (2-20 nm) formed at 12h has resulted in the highest strength development, which suggests that this facile hydrothermal method can be conducted to prepare a tough and porous diatomite-based adsorbent simultaneously.

A detailed investigation of the difference in microstructure between raw diatomite and the hydrothermally hardened (12 M NaOH, 12 h, 473 K) diatomite-based adsorbent was conducted using nitrogen gas sorption analysis (Figure 14). The BET surface areas and total pore volumes obtained for the two specimens were 40.25 $m^2 \cdot g^{-1}$ and 0.0848 $cm^3 \cdot g^{-1}$, and 74.42 $m^2 \cdot g^{-1}$ and 0.192 $cm^3 \cdot g^{-1}$, respectively, suggests that the formation of analcime could improve the porosity of the diatomite-based adsorbent obviously. For

the synthesized diatomite-based adsorbent, a Type-IV isotherm was observed (according to the IUPAC classification) with H3-type hysteresis, which behaves characteristic of a mesoporous or macroporous material where the pores are slit-like or aggregates of plate-like particles.[31] This also explains the strengthening effect with analcime formation described above. In addition to its highly porous structure with three dimensional frameworks, analcime usually has a negative charge, and the negative charge can be balanced by cations which are exchangeable with certain cations (e.g. heavy metals) in solutions.[1] The CEC test also revealed that the formed diatomite-based materials has a better cation-exchange capacity (66.5 $cmol^{+}\cdot kg^{-1}$) than that of diatomite (24.9 $cmol^{+}\cdot kg^{-1}$), which indicates that the diatomite-based adsorbent are applicable in removing contaminants such as heavy metals and dyes in solutions.

3.3. Adsorption of MB

The performance of the synthesized adsorbent for MB capture was tested at different dye concentrations (250, 500, and 1000 ppm) and temperatures (288, 298 and 308 K) respectively. Figure 15 shows that the adsorption capacity increases with increasing both the initial MB concentration and the temperature, suggesting that the adsorption process belongs to endothermic.

3.3.1. Adsorption Isotherms.

Adsorption isotherms reveal the interaction mechanism between molecular adsorbate and solid adsorbents at equilibrium. The data recorded in this work were modeled

assuming either the Langmuir or Freundlich equation. The former is usually appropriate for ideal monolayer adsorption. The (linear) Langmuir equation is

$$\frac{C_e}{q_e} = \frac{1}{q_{\max} K_L} + \frac{C_e}{q_{\max}} \tag{3}$$

where $q_{\max}$ (mg·g^{-1}) is the maximum adsorption capacity, K_L (L·mg^{-1}) is the Langmuir constant related to the enthalpy of the process, and the other symbols are defined as above. The Freundlich equation is an empirical model describing heterogeneous adsorption processes; its linear form is

$$\ln q_e = \ln K_F + \frac{1}{n} \ln C_e \tag{4}$$

where K_F is the Freundlich constant, related to the adsorption capacity of the adsorbent, and n is the Freundlich exponent, which varies with the adsorption intensity and reveals the surface heterogeneity of the adsorbent. Table 1 lists the adsorption parameters obtained here for the adsorption of MB onto the diatomite-based specimens. The higher coefficients of determination (R^2) obtained with the Langmuir model indicate that the adsorption process is best characterized by the formation of a monolayer distribution of MB molecules on the homogeneous active surface of the diatomite-based adsorbent, and no interaction exist between the adsorbed MB molecules. Table 1 also shows that $q_{\max}$, the adsorption capacity for MB of the synthesized material, increases with increasing temperature with a maximum adsorption capacity of 129.87 mg·g^{-1} at 308 K. It is noticeable that the synthesized diatomite-based adsorbent showed higher or

comparable adsorptive capacity when compared with other natural clays (Table 2), zeolites or commercial/chemically synthesized zeolite reported previously, indicating that the material synthesized here is a more efficient adsorbent.

3.3.2. Adsorption Kinetics.

The experimental data obtained at 298 K and at different MB concentrations were fit using the well-known pseudo-first-order and pseudo-second-order kinetic models, namely

$$\ln(q_e - q_t) = \ln q_e - k_1 t \quad (5)$$

and

$$\frac{t}{q_t} = \frac{1}{k_2 q_e^2} + \frac{t}{q_e} \quad (6)$$

where q_e and q_t (mg·g^{-1}) are the amounts of MB adsorbed at equilibrium and at a given time (t, h), and k_1 (h^{-1}) and k_2 (g·mg^{-1}·h^{-1}) are respectively the first- and second-order rate constants. The values obtained with both models are listed in Table 3.

The pseudo-second-order model provides better fits (higher R^2 statistics) for all initial MB concentrations, and yields q_e values are much closer to those measured experimentally. This implies that the adsorption of MB onto the synthesized diatomite-based material proceeds via chemisorption.[32]

3.3.3. Adsorption Thermodynamics.

The thermodynamic parameters for the adsorption process were determined from the experimental data using the following equations:

$$K_d = \frac{C_0 - C_e}{C_e}\frac{V}{M} \tag{7}$$

$$\ln K_d = \frac{\Delta S}{R} - \frac{\Delta H}{RT} \tag{8}$$

and

$$\Delta G = \Delta H - T\Delta S \tag{9}$$

where R (8.314 J·mol^{-1}·K^{-1}) is the ideal gas constant, H is the enthalpy, S is the entropy, and G is the Gibbs free energy, and the other symbols are defined as above.

The positive values obtained for ΔS (Table 4) suggest that the affinity of the adsorbent for MB is the result of increased randomness at the interface between the solid and liquid phases during adsorption.[32] The positive ΔH shows that this process is endothermic. The decrease in G—with more negative values determined for ΔG at higher temperatures shows that the adsorption process is spontaneous (energetically favorable) and becomes even more effective as the temperature increased.

4. CONCLUSIONS

A novel hardened diatomite-based adsorbent with zeolite formation has been synthesized hydrothermally from natural diatomite, and furthermore its adsorption behavior for MB has also been investigated. The experimental results can be summarized as follows:

(i) A tough and porous adsorbent could be synthesized hydrothermally with diatomite. The initial strength was provided with the formed C-S-H gel, while the final strength development came from the zeolite (analcime) formation. The both formed C-S-H gel and analcime not only could improve the strength, but only could enhance the adsorption of MB. The NaOH addition had a significant effect on the C-S-H and analcime formations, and at a lower NaOH concentration (≤9 M), C-S-H gel favored to form, while at higher NaOH concentration (≥12 M) analcime could form. The curing temperature and time also influenced the formation of analcime, a long curing time (≥12 h) or a high temperature (≥473 K) was favorable to analcime formation, while an overlong time (≥24h) or over-high temperature (≥493 K) led to a decrease in the strength of the specimens. Due to the low temperature synthesis, the formed analcime and retained diatomite were found to exert a synergistic effect on MB adsorption.

(ii) The adsorption of MB by the synthesized diatomite-based material was well modeled by a Langmuir process (R^2 > 0.99), with a maximum monolayer adsorption capacity of 129.87 $mg \cdot g^{-1}$ at 308 K. The kinetics of the process could be described by the pseudo-second-order model, with the associated thermodynamic parameters showing that the adsorption is endothermic (positive ΔH) and spontaneous (negative ΔG).

AUTHOR INFORMATION

Corresponding Author

*E-mail: zzjing@tongji.edu.cn

Author Contributions

The manuscript was written through contributions of all authors. All authors have given approval to the final version of the manuscript.

Notes

The authors declare no competing financial interests.

ACKNOWLEDGEMENTS

This study was financially supported by the National Natural Science Foundation of China (Grant Nos. 51072138 and 51272180) and was also supported by the Yoshioka Laboratory of the Graduate School of Environmental Studies of Tohoku University.

Reference

1. M. T. Yagub, T. K. Sen, S. Afroze and H. M. Ang, *Advances in Colloid and Interface Science*, 2014, **209**, 172-184.
2. M. A. Al-Ghouti, Y. S. Al-Degs, M. A. M. Khraisheh, M. N. Ahmad and S. J. Allen, *Journal of Environmental Management*, 2009, **90**, 3520-3527.
3. M. Rafatullah, O. Sulaiman, R. Hashim and A. Ahmad, *Journal of Hazardous Materials*, 2010, **177**, 70-80.
4. J. Zhu, Y. Wang, J. Liu and Y. Zhang, *Industrial and Engineering Chemistry Research*, 2014, **53**, 13711-13717.
5. K. Mukherjee, A. Kedia, K. J. Rao, S. Dhir and S. Paria, *Rsc Adv*, 2015, **5**, 30654-30659.
6. V. R. Pereira, A. M. Isloor, U. K. Bhat, A. F. Ismail, A. Obaid and H. K. Fun, *Rsc Adv*, 2015, **5**, 53874-53885.
7. M. L. Weng, Z. J. Zhou and Q. Zhang, *Int J Electrochem Sc*, 2013, **8**, 290-296.
8. R. Khan, P. Bhawana and M. H. Fulekar, *Rev Environ Sci Bio*, 2013, **12**, 75-97.
9. W. Yu, L. Deng, P. Yuan, D. Liu, W. Yuan and F. Chen, *Chemical Engineering Journal*, 2015, **270**, 450-458.
10. A. F. Danil de Namor, A. El Gamouz, S. Frangie, V. Martinez, L. Valiente and O. A. Webb, *J Hazard Mater*, 2012, **241-242**, 14-31.
11. S. Wang and Y. Peng, *Chemical Engineering Journal*, 2010, **156**, 11-24.
12. Z. Ioannou, C. Karasavvidis, A. Dimirkou and V. Antoniadis, *Water science and technology : a journal of the International Association on Water Pollution Research*, 2013, **67**, 1129-1136.
13. O. Hernandez-Ramirez, P. I. Hill, D. J. Doocey and S. M. Holmes, *Journal of Materials Chemistry*, 2007, **17**, 1804-1808.
14. C. R. Nascimento, E. M. O. Sobrinho, R. B. Assis, R. F. Fagundes, L. Bieseki and S. B. C. Pergher, *Ceramica*, 2014, **60**, 63-68.
15. N. van Garderen, F. J. Clemens, M. Mezzomo, C. P. Bergmann and T. Graule, *APPLIED CLAY SCIENCE*, 2011, **52**, 115-121.
16. W. N. Shen, L. J. Feng, A. Lei and M. J. Guo, *Advanced Materials and Process Technology, Pts 1-3*, 2012, **217-219**, 879-885.
17. E. H. Ishida, *Soil-ceramics (Earth), self-adjustment of humidity and temperature. In:Schwartz M, editor. Encyclopedia of Smart Materials*, Wiley, New York, 2002.
18. L. Zhou, Z. Z. Jing, Y. Zhang, K. Wu and E. H. Ishida, *Applied Clay Science*, 2012, **69**, 30-36.
19. K. Wu, Z. Z. Jing, L. L. Pan, L. Zhou and E. H. Ishida, *Res Chem Intermediat*, 2012, **38**, 1637-1646.
20. Y. Zhang, Z. Z. Jing, X. W. Fan, J. J. Fan, L. Lu and E. H. Ishida, *Industrial & Engineering Chemistry Research*, 2013, **52**, 4779-4786.
21. S. D. Miao, Z. M. Liu, H. W. Ma, B. X. Han, J. M. Du, Z. Y. Sun and Z. J. Miao, *Microporous and Mesoporous Materials*, 2005, **83**, 277-282.
22. X. Ma, J. Yang, H. Ma, C. Liu and P. Zhang, *Microporous and Mesoporous Materials*, 2015, **201**, 134-140.

23. G. Garcia, E. Cardenas, S. Cabrera, J. Hedlund and J. Mouzon, *Microporous and Mesoporous Materials*, 2016, **219**, 29-37.
24. P. Djomgoue and D. Njopwouo, *Journal of Surface Engineered Materials and Advanced Technology*, 2013, **3**, 275.
25. G. Sheng, J. Hu and X. Wang, *Applied radiation and isotopes*, 2008, **66**, 1313-1320.
26. Y. Al-Degs, M. A. M. Khraisheh and M. F. Tutunji, *Water Research*, 2001, **35**, 3724-3728.
27. P. Laoot, K. Rangsriwatananon and A. Chaisena, *JOURNAL OF CERAMIC PROCESSING RESEARCH*, 2011, **12**, 273-278.
28. M. Sprynskyy, T. Kowalkowski, H. Tutu, E. M. Cukrowska and B. Buszewski, *Colloids and Surfaces A: Physicochemical and Engineering Aspects*, 2015, **465**, 159-167.
29. Y. Jing, Z. Jing and E. H. Ishida, *Industrial and Engineering Chemistry Research*, 2013, **52**, 17865-17870.
30. Z. Z. Jing, F. M. Jin, N. Yamasaki, H. Maeda and E. H. Ishida, *Journal of Environmental Management*, 2009, **90**, 1744-1750.
31. W. Wang, G. Tian, Z. Zhang and A. Wang, *Chemical Engineering Journal*, 2015, **265**, 228-238.
32. L. Zheng, C. Wang, Y. Shu, X. Yan and L. Li, *Colloids and Surfaces A: Physicochemical and Engineering Aspects*, 2015, **468**, 129-139.
33. A. Gucek, S. Sener, S. Bilgen and M. A. Mazmanci, *Journal of Colloid and Interface Science*, 2005, **286**, 53-60.
34. A. Al-Futaisi, A. Jamrah and R. Ai-Hanai, *Desalination*, 2007, **214**, 327-342.
35. C. D. Woolard, J. Strong and C. R. Erasmus, *Appl Geochem*, 2002, **17**, 1159-1164.
36. J. Zhang, Q. W. Ping, M. H. Niu, H. Q. Shi and N. Li, *Applied Clay Science*, 2013, **83-84**, 12-16.
37. R. P. Han, J. J. Zhang, P. Han, Y. F. Wang, Z. H. Zhao and M. S. Tang, *Chemical Engineering Journal*, 2009, **145**, 496-504.
38. W. T. Tsai, K. J. Hsien and H. C. Hsu, *Journal of Hazardous Materials*, 2009, **166**, 635-641.
39. Z. Sun, C. Li and D. Wu, *Journal of Chemical Technology and Biotechnology*, 2010, **85**, 845-850.

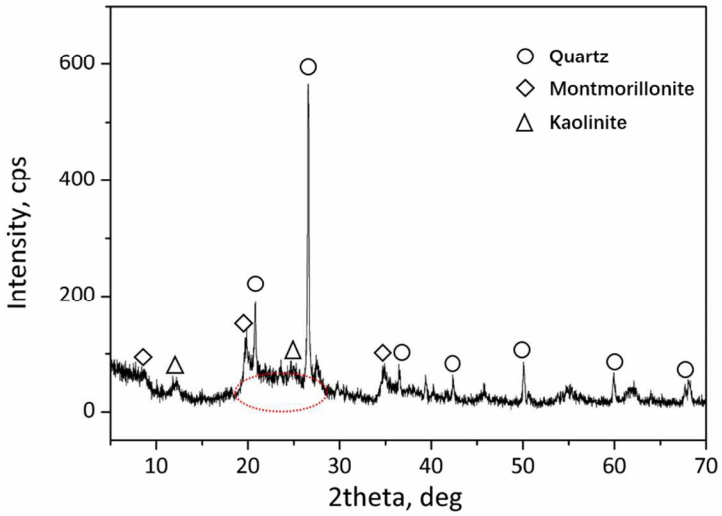

Figure 1. The XRD pattern of natural diatomite.

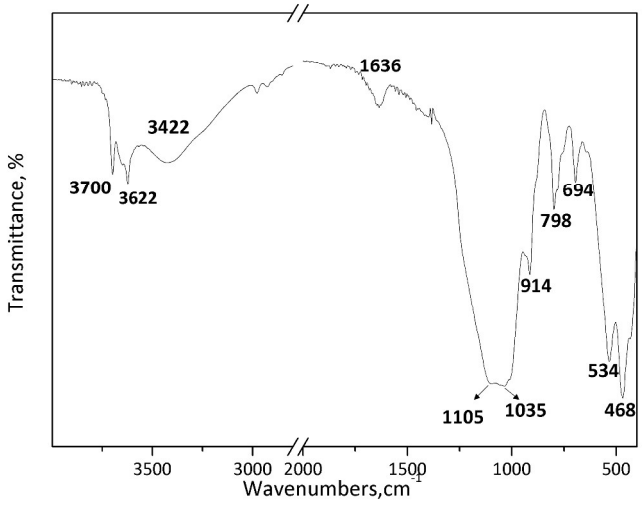

Figure 2. The FTIR spectra of natural diatomite.

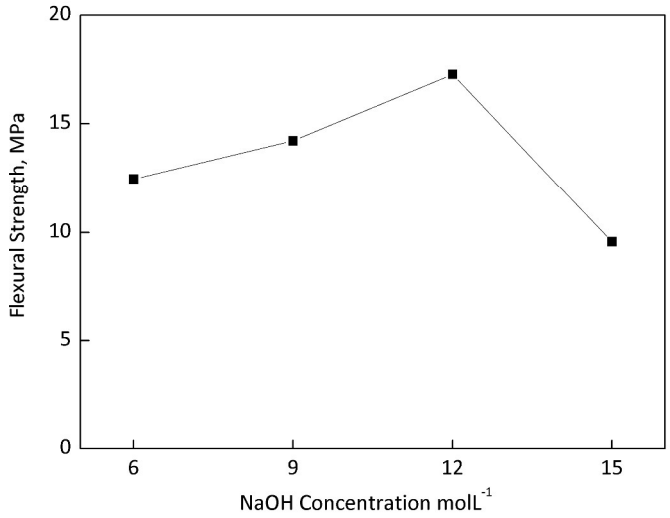

Figure 3. Flexural strength development of specimens hydrothermally synthesized from diatomite at 473 K for 12h with different NaOH concentrations.

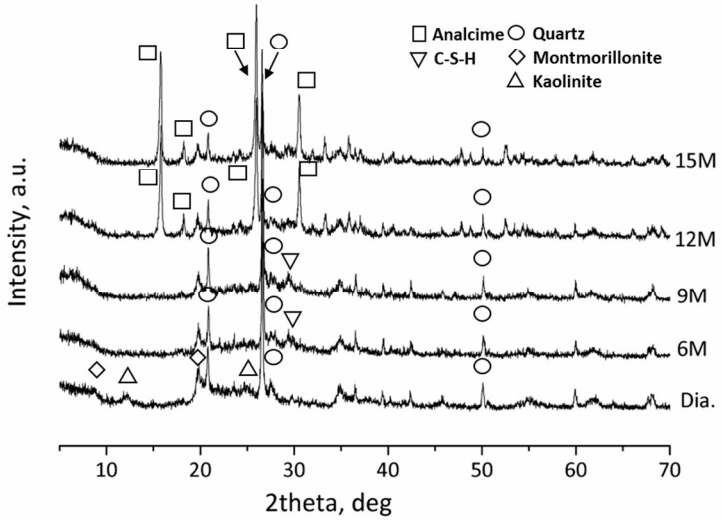

Figure 4. XRD patterns of synthesized specimens cured at 473K for 12h with different NaOH concentrations.

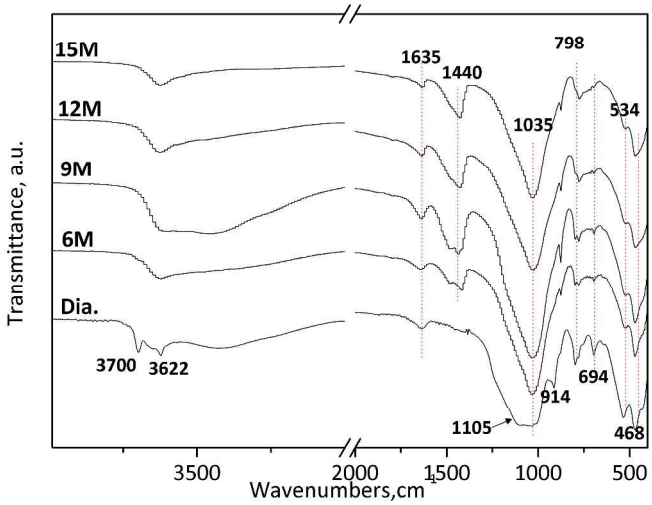

Figure 5. FTIR spectra of synthesized specimens cured for 12h at 473K with different NaOH concentrations.

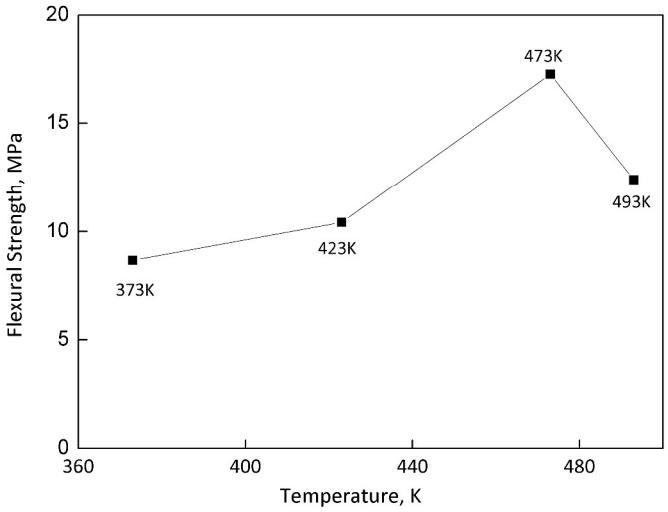

Figure 6. Flexural strength development of specimens synthesized from diatomite with 12 M NaOH for 12 h at different temperatures.

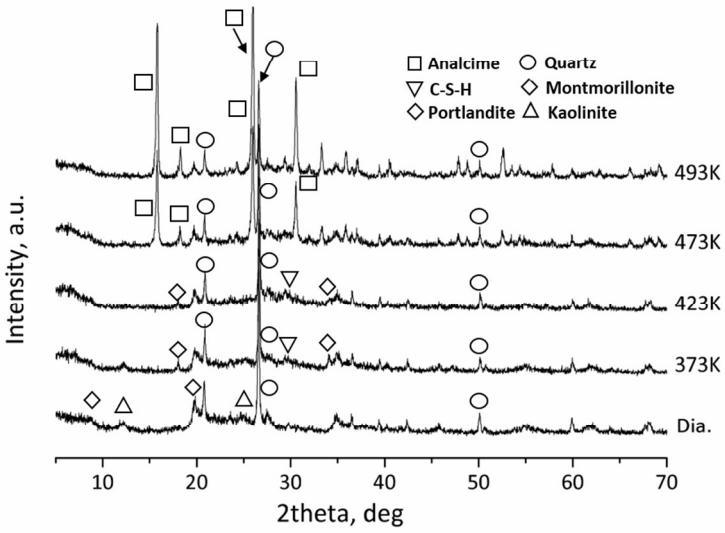

Figure 7. X-ray diffraction patterns of specimens hydrothermally synthesized from diatomite for 12 h with 12 M NaOH at different temperatures.

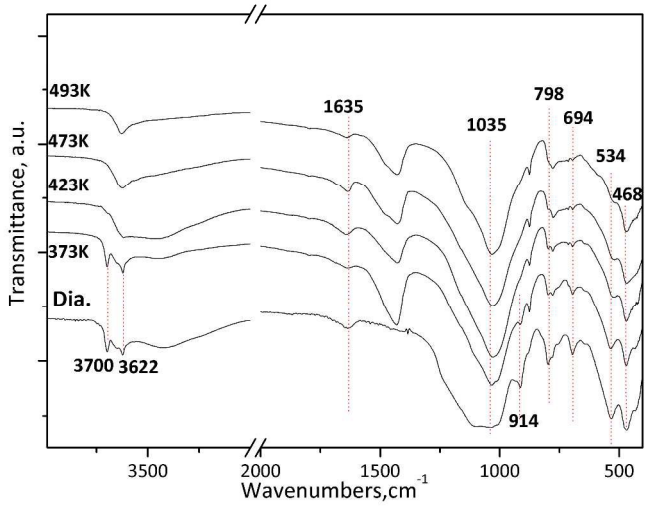

Figure 8. FTIR spectra of specimens with 12M NaOH, cured for 12h at different temperatures.

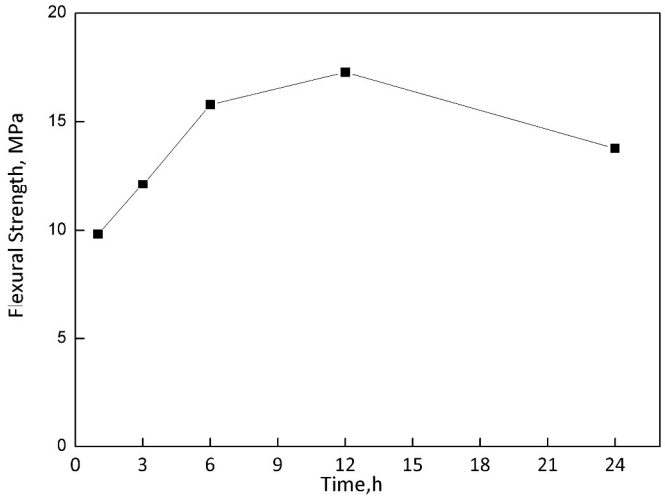

Figure 9. Flexural strength development of specimens synthesized from diatomite with 12 M NaOH at 473 K for different times.

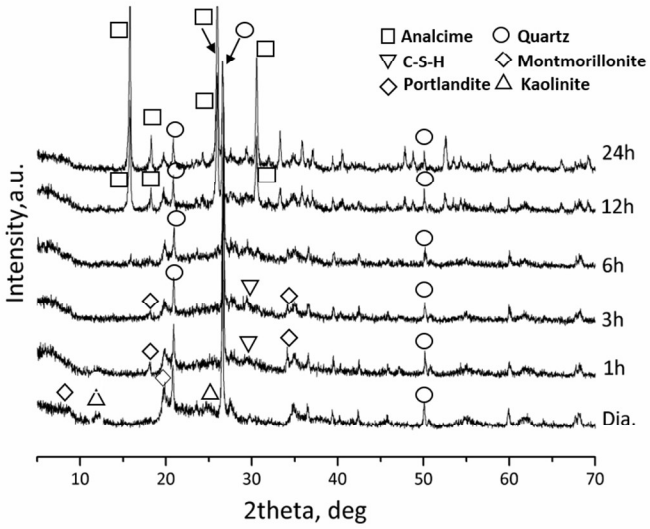

Figure 10. X-ray diffraction patterns of specimens hydrothermally synthesized from diatomite at 473 K with 12 M NaOH for different times.

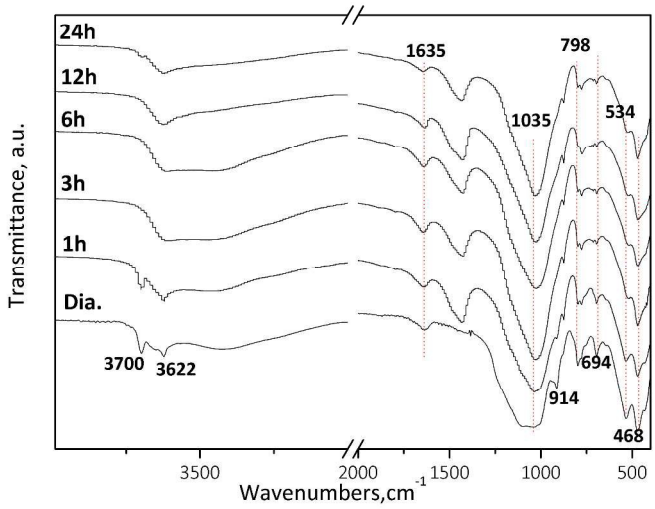

Figure 11. FTIR spectra of adsorbents of the synthesized specimens from diatomite at 473 K with 12 M NaOH for different times.

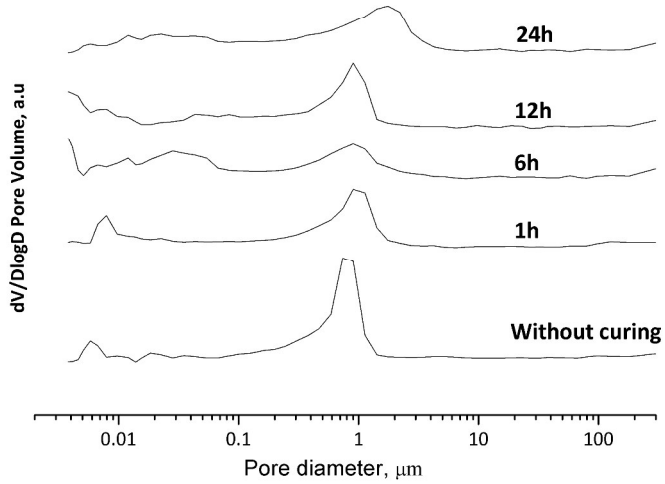

Figure 12. Evolution of the pore size distribution of specimens cured at 473K for different curing times.

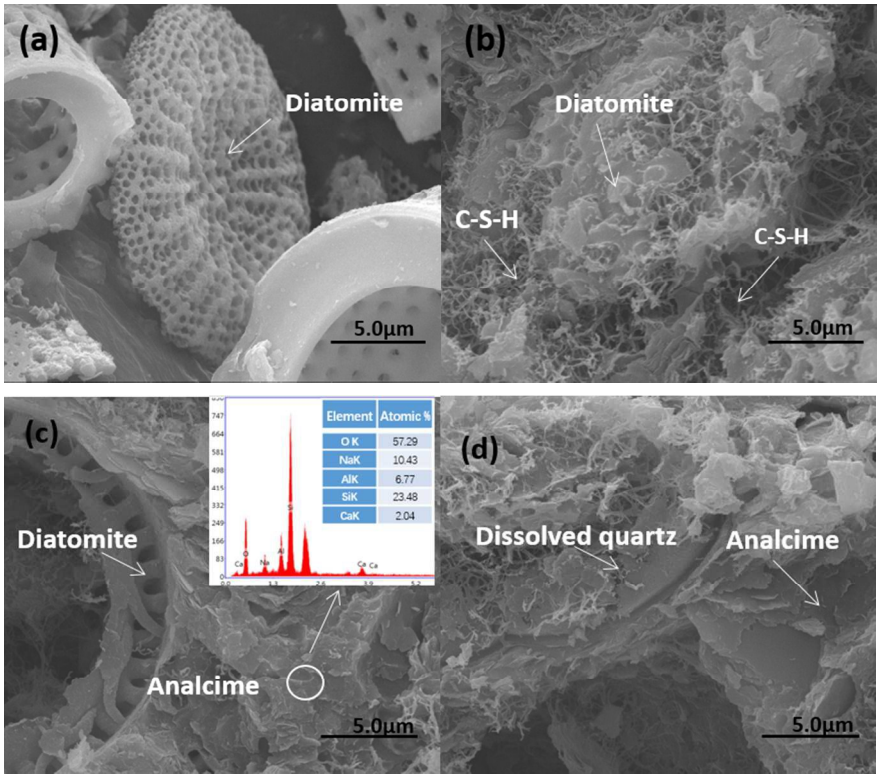

Figure 13. SEM micrographs of (a) diatomite and the diatomite-based specimen synthesized at 473 K with 12 M NaOH for (b) 6h, (c)12h, and (d) 24h respectively.

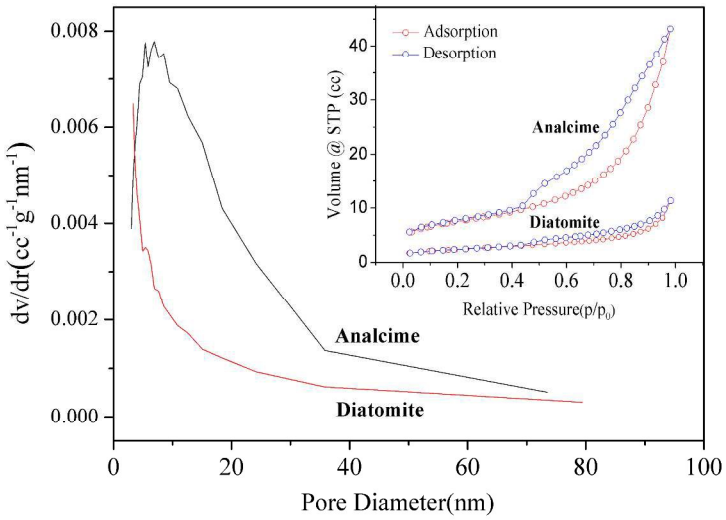

Figure 14. Pore size distributions, calculated using the Barrett-Joyner-Halenda method, for raw diatomite and the diatomite-based specimen synthesized with 12 M NaOH for 12 h at 473 K. The inset shows the corresponding N_2 adsorption-desorption isotherms.

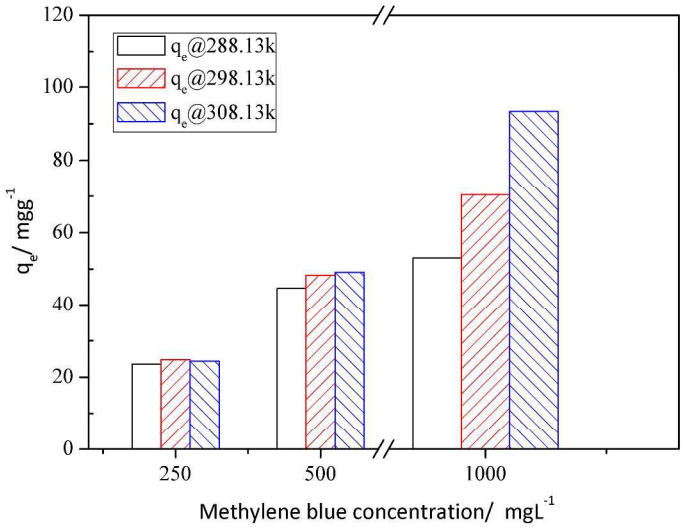

Figure 15. Equilibrium capacities for MB, at different temperatures and concentrations, of the diatomite-based specimen hydrothermally synthesized at 473 K for 12 h with12 M NaOH.

Table 1. Adsorption isotherm of MB onto the Synthesized diatomite-based Material

T (K)	Langmuir model			Freundlich model		
	q_{max} (mg·g^{-1})	K_L (L·mg^{-1})	R^2	K_F	n	R^2
288.15	54.95	0.0616	0.9998	14.969	4.57	0.7953
298.15	72.99	0.0877	0.9997	18.433	4.05	0.8002
308.15	129.87	0.0392	0.9934	9.765	1.82	0.9511

Table 2. Comparison of the maximum adsorption capacities of MB by diatomite-based adsorbent with literature values for other clay and zeolites

Adsorbents	Adsorption capacity (mg g^{-1})	sources
Pyrophyllite	70.4	[33]
Palygorskite	50.8	[34]
Amorphous silica	22.7	[35]
Diatomite	1.7	[36]
Modified diatomite	18.1	[36]
Natural zeolite(China)	16.4	[37]
Zeolite-P2(purely synthesized)	16.9	[38]
Zeolite(synthesized)	50.5	[39]

Table 3. Adsorption kinetics of Methylene Blue onto the Synthesized diatomite-based Material at 298 K

C_i (ppm)	q_e[a] (mg·g^{-1})	Pseudo-first order model			Pseudo-second order model		
		q_e[b] (mg·g^{-1})	k_1 (h^{-1})	R^2	q_e[b] (mg·g^{-1})	k_2 (g·mg^{-1}·h^{-1})	R^2
250	24.78	13.34	0.103	0.9837	25.58	0.0189	0.9997
500	48.31	30.62	0.0464	0.9874	50.00	0.00436	0.9947
1000	70.44	43.89	0.0404	0.9832	72.46	0.00157	0.9888

[a]experimental values, [b]calculated values

Table 4. Thermodynamics of MB Adsorption onto diatomite-based Material

C_i (ppm)	ΔH (kJ·mol^{-1})	ΔS (J·mol^{-1}·K^{-1})	ΔG (kJ·mol^{-1})		
			288.15 K	298.15 K	308.15 K
250	32.27	174.14	−17.91	−19.65	−21.39
500	54.17	245.20	−16.48	−18.93	−21.38
1000	92.62	359.21	−10.88	−14.47	−18.07

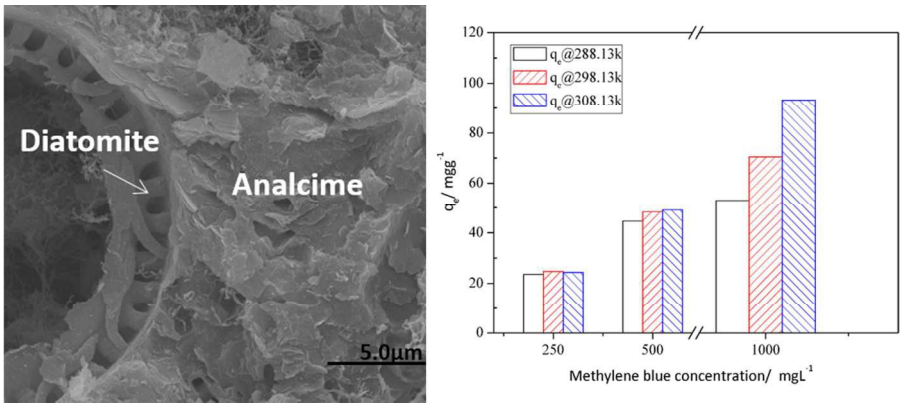

Graphical Abstract: a tough diatomite-based adsorbent with analcime formation was synthesized hydrothermally and used to capture methylene blue efficiently.